Photodissociation Spectroscopy of Cold Protonated Synephrine: Surprising Differences Between IR-UV Hole-Burning and IR Photodissociation Spectroscopy of the O-H and N-H modes

N. Nieuwjaer, C. Desfrançois, F. Lecomte, B. Manil, S. Soorkia, M. Broquier, Gilles Grégoire

Photodissociation Spectroscopy of Cold Protonated Synephrine: Surprising Differences Between IR-UV Hole-Burning and IR Photodissociation Spectroscopy of the O-H and N-H modes

N. Nieuwjaer,[a] C. Desfrançois,[a] F. Lecomte,[a] B. Manil,[a] S. Soorkia,[b,c] M. Broquier,[b,c] and G. Grégoire[*,b,c]

[a] Laboratoire de Physique des Lasers, CNRS, Université Paris 13, Sorbonne Paris Cité, 93430 Villetaneuse, France.

[b] Institut des Sciences Moléculaires d'Orsay (ISMO), CNRS, Univ. Paris Sud, Université Paris-Saclay, F-91405 Orsay (France)

[c] Centre Laser de l'Université Paris-Sud (CLUPS/LUMAT), Univ. Paris-Sud, CNRS, IOGS, Université Paris-Saclay, F-91405 Orsay (France)

Corresponding author :

* Email : gilles.gregoire@u-psud.fr Tel (33) 1 6915 3103

Abstract

We report the UV and IR photofragmentation spectroscopies of protonated synephrine in a cryogenically cooled Paul trap. Single (UV or IR) and double (UV-UV and IR-UV) resonance spectroscopies have been performed and compared to quantum chemistry calculations, allowing the assignment of the lowest-energy conformer with two rotamers depending on the orientation of the phenol hydroxyl (OH) group. The IR-UV Hole Burning spectrum exhibits the four expected vibrational modes in the 3 µm region, *i.e.* the phenol OH, C_β-OH and two NH_2^+ stretches. The striking difference is that among these modes, only the free phenol OH mode is active through IRPD. The protonated amino group acts as a proton donor in the internal hydrogen bond and displays large frequency shifts upon isomerization expected during the multiphoton absorption process, leading to the so-called IRMPD transparency. More interestingly, while the C_β-OH is a proton acceptor group with moderate frequency shift for the different conformations, this mode is still inactive through IRPD.

1. Introduction

Synephrine is an alkaloid that is naturally contained in some plants.[1] It is one of the most popular stimulants present in weight-loss products, becoming the main substitute of ephedrine after this latter was banned in dietary products by the Food and Drug Administration in the United States of America. The effects of synephrine are close to those of caffeine or ephedrine: increase of blood pressure and heart rate. It is used pharmacologically as a sympathomimetic agent, with vasoconstrictor and bronchiectatic agent. The neurotransmitter adrenaline is the catechol analogue of synephrine. Synephrine indeed activates several types of adrenergic receptors[2,3] as the catechol amines. In the signaling process, synephrine is recognized by G protein-coupled receptors. This binding process induces geometric changes in the receptor protein, which regulates its activities. Since the receptor protein recognizes the shapes of the signalization molecule, synephrine flexibility is an essential property of this allosteric effect. The conformational geometries of neutral synephrine have been investigated by gas-phase optical spectroscopies by M. Fujii *et al.*[4] Nevertheless, synephrine is protonated at physiological conditions (pKa=9.15) and could adopt several conformations as the catechol amines, with (or without) an interaction of the protonated moieties with the aromatic ring (folded conformer). Studying cold protonated molecules through laser spectroscopy techniques in the gas phase indeed allows assigning their structures through comparison with quantum chemical calculations. Recently, cold protonated noradrenaline has been investigated through laser (UV and IR-UV) photodissociation spectroscopy by M. Fujii *et al*.[5] They have shown that two main types of conformations coexist at low temperature (15 K), the lowest energy folded conformer and an extended structure in which the protonated amino group does not interact with the catechol ring. At the low temperature of the cold Paul trap, the extended conformation was not expected to be significantly populated while being clearly observed, underlying a possible kinetic trapping of this conformation initially present in solution.

For the last decade, gas phase action spectroscopy has been largely employed to assign the structure of biomolecular ions through IRMPD technique.[6–8] The high brightness and temporal profile of free electron laser (FEL) pulses (train consisting of hundreds of picosecond pulses within a macro pulse of about 10 µs) is particularly well suitable for non-coherent sequential multiphoton absorption process, following each time by internal vibrational redistribution

(IVR), as required to induce photofragmentation of any molecular ions with low energy mid-IR photons (500-2000 cm^{-1}). More recently, IR photodissociation of gaseous ions using tabletop nanosecond OPO IR lasers (denoted IRPD hereafter) has been developed mostly to cover the high frequency spectral region around 3 µm that can hardly be reached by FEL. A tabletop IR laser normally runs at 10 Hz and delivers 10 ns pulses at a much lower power than a FEL. At the beginning, only jet-cooled non-covalent ionic complexes or rare-gas tagged ions[9–12] were investigated through IRPD mostly because the energy brought by a single IR photon can overcome the low dissociation energy of these complexes. Although in linear or Paul traps, the laser can be shined for hundreds of milliseconds to seconds, the increase of internal energy needed to induce fragmentation can only be obtained within one single pulse before thermalization by collisions with the He buffer gas loaded in the trap. High-energy laser, typically in the order of 10-25 mJ/pulse are then used to enhance multiphoton absorption within one laser shot. With FT-ICR, the very low backing pressure in the cell allows for the continuous increase of internal energy through multiple absorption at each laser pulse, increasing the photofragmentation signal.[13] In any case, due to the anharmonicity bottleneck, coherent multiphoton absorption cannot occur, so fast IVR process is required to increase the internal energy until dissociation.

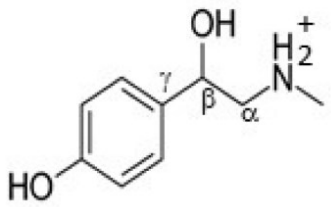

Chart 1 : Structure of protonated synephrine $SyneH^+$.

More recently, UV photofragmentation spectroscopy of cold molecular ions has emerged as a promising tool to probe the conformational heterogeneity of biomolecules. Conformer selectivity indeed relies on the high sensitivity of the electronic states to the local interaction of the aromatic chromophore. In some cases, specific photofragments, *i.e.* not those commonly detected through slow heating methods in the ground state (either through CID or IR), are detected, allowing a rapid and efficient screening of the conformation of the molecules.[14] For midsize systems, *ab initio* quantum chemical calculations can accurately

reproduce the experimental vibronic spectra leading to conformer assignment.[15,16] Besides, IR-UV[5,17,18] and UV-UV[19–22] double resonance spectroscopies of cold ions have been developed as done for decades to study neutral molecules streamed in a cold supersonic expansion.

In this paper, we study the cold protonated synephrine ion, $SyneH^+$ (chart 1), isolated in the gas phase, with the help of a combination of UV, UV-UV, IR-UV and IR photofragmentation spectroscopies and quantum chemistry calculations. UV-UV Hole Burning (HB) spectroscopy is used to discriminate and assign the ion structures while the corresponding IR spectra are obtained either from IR-UV HB spectroscopy or from direct IRPD. In the former case, IR absorption is monitored by a one-photon depletion process in the fragment ion signal while, in the latter case, the IR spectra results from a sequential absorption of few photons within the IR laser pulse, with enough energy gain for ion fragmentation. UV spectroscopic results are compared with quantum chemistry calculations of the equilibrium geometry of the ground and excited electronic states. IR-UV and IRPD spectra are compared with each other and with normal-mode frequencies and intensities calculated for the different conformers.

2. Experimental and theoretical methods

The overall setup installed at the Laser Center Facility in Orsay (CLUPS) has already been described in details.[22] Briefly, Synephrine (Sigma Aldrich) is dissolved in water/methanol mixtures (50/50 by volume) at 100 μM and together with few droplets of acetic acid. $SyneH^+$ ions are produced in an electrospray source and the ions are first stored in an octopole ion trap for 100 ms, extracted and accelerated at 220 V by a pulsed exit electrode and then transferred in the 3D-QIT (Jordan Tof Inc.). The latter is biased at 220 V to ensure efficient trapping and avoid collision induced dissociation of the incoming ions with He buffer gas injected by a pulsed valve 1-2 ms before. The 3D-QIT is housed in a copper box directly mounted on a cold head of a compressed helium cryostat that maintains the temperature around 10-15 K. A pulsed mass gate located before the entrance of the trap allows for mass-selecting the parent ion. The photodissociation laser is triggered after 40 ms when thermalization of the protonated ions is fully achieved and helium buffer gas is pumped. All ionic fragments and parent molecules are then extracted and accelerated for mass-analysis in a linear time-of-flight mass spectrometer and detected by MCP (Z-Gap, Jordan Tof Inc.).

The UV photodissociation laser is the output of a frequency doubled dye laser (Quantel TDL 90), pumped by the second harmonic of a YAG laser (Quantel YG980), which resolution is about 0.2 cm^{-1}. UV-UV HB spectroscopy has been performed following the method we have already presented.[22] The probe laser is scanned and triggered within the rising time of the extraction pulse of the QIT (350 V, rise time of 80 ns), so a given ionic fragments is less accelerated than in normal conditions (with the burn laser set to a vibronic transition of a given conformer and triggered any time before the extraction pulse), which leads to two different times-of-flight for the same m/z. In order to increase the UV-UV HB signal-to-noise ratio, we run the burn laser at 5 Hz while keeping the probe at 10 Hz and perform the experiment using the modified active baseline subtraction methods.

For the IR-UV HB experiments, the UV wavelength is set to a vibronic transition of a given conformer while the IR laser is scanned from 3100 cm^{-1} to 3750 cm^{-1}, 100 ns before the UV laser. Resonant absorption of one IR photon results in a ground state depopulation and thus a dip in the UV photofragmentation yield. The IR laser is the output of an KTP-based OPO (Euroscan) pumped by a 10 Hz Nd:YAG (Quantel YG980). Typical energy per pulse is of the order of 100 µJ over the whole spectral range, with a maximum of 150 µJ around 3 µm and a spectral resolution of 3 cm^{-1}. The IR beam is focused in the center of the trap with a CaF_2 lens (focus length of 2000 mm or 350 mm) for the IR-UV or IRPD spectroscopy, respectively.

Ab initio calculations have been performed with the TURBOMOLE program package (v6.6)[23] making use of the resolution-of-the-identity (RI) approximation for the evaluation of the electron-repulsion integrals.[24] The equilibrium geometries of $SyneH^+$ in its electronic ground (S_0) and excited (S_1 and more) states have been determined at the CC2 level[25] with the correlation-consistent polarized valence double-ζ aug-cc-pVDZ basis set augmented with diffuse functions.[26] The vibrational modes of the ground and the first excited states have been calculated at the same level in order to obtain the adiabatic excitation energy corrected for the difference of zero-point energy between the two states. Finally, the ground-state vibrational spectra have been simulated at the RI-DFT/B97-D3/TZVPP level[27,28] with the dispersion correction D3 of Grimme.[29] The harmonic frequencies are corrected with a global scaling factor of 0.9744[30] for all modes.

3. Results and Discussion

3. 1. Experimental Spectra

The UV excitation of SyneH$^+$ (m/z 168) results in fragmentation through C_α-C_β bond cleavage, leading to m/z 125 and m/z 44 – 46, depending on the final localization of the charge and hydrogens, and C_β-C_γ bond cleavage leading to m/z 95 (Figure S1). The photofragmentation efficiency is rather weak, in the order of few %, and the fragmentation branching ratio is constant over the probed spectral range. These fragments are specific of electronic excitation whereas water loss (m/z 150) is the main fragment obtained through collision induced dissociation or direct IR photodissociation (IRPD) around 3 µm (see Figure S1).

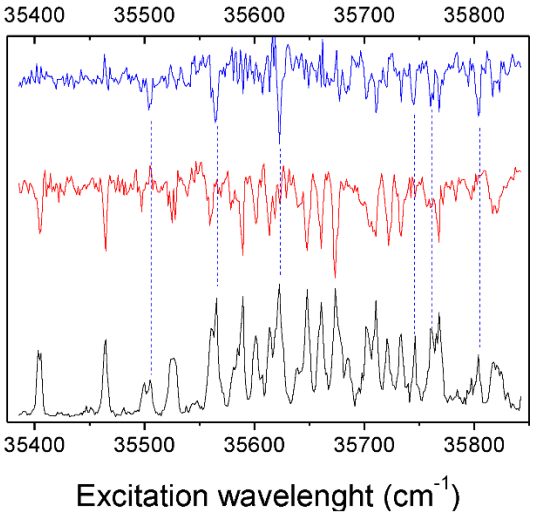

Figure 1. Bottom trace: UV photodissociation spectrum of SyneH$^+$ (black line). Top traces: UV-UV HB spectra with the burn laser set at the band origin of the two conformers at 35 406 cm^{-1} (red line) and 35 509 cm^{-1} (blue line).

The vibronic UV spectrum of SyneH$^+$, averaged on the signal of all ionic fragments, is reported in Figure 1, bottom trace, from 35 400 cm^{-1} to 35 850 cm^{-1}. As it can be readily checked, a dense vibronic progression is observed, with a first transition recorded at 35 406 cm^{-1}. A first UV-UV HB spectrum has thus been recorded by setting the burn laser frequency at this first transition (top trace, red line), which accounts for most of the vibronic transitions detected in the 1-color spectrum. A second UV-UV HB spectrum is obtained by setting the burn laser at the first missing transition at 35 509 cm^{-1} (top trace, blue line). The two UV-UV HB spectra allow recovering the entire vibronic spectrum of SyneH$^+$, which clearly reveals that only two

conformers contribute to the experimental spectrum in that spectral region. The energy splitting of the band origins of the two conformers is 103 cm^{-1}.

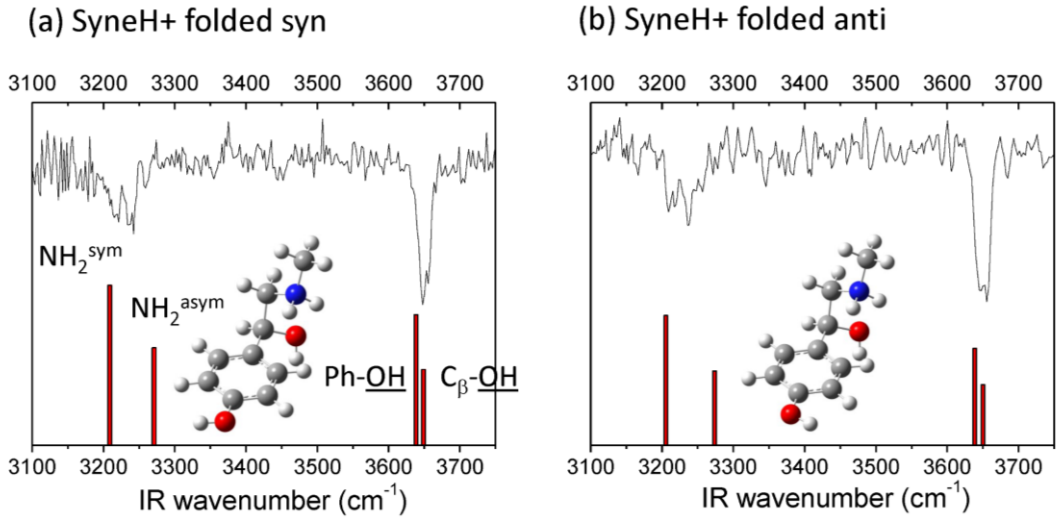

Figure 2. IR-UV HB spectra of (a) rotamer syn (b) rotamer anti of the lowest energy conformer of $SyneH^+$ compared to their calculated harmonic frequencies (DFT/B97-D3/TZVPP) scaled by 0.9744. Signals at the hydroxyl mode frequencies correspond to a saturated 50% depletion.

IR-UV HB spectroscopy has been performed to record the conformer-selected vibrational spectra of $SyneH^+$. The two IR HB spectra are obtained by scanning the IR frequencies while probing the photofragmentation signal with UV wavelength set at the band origin of the two conformers found with the UV-UV HB spectroscopy. The two spectra are reported in Figure 2 from 3100 cm^{-1} to 3800 cm^{-1}. They are almost identical within the experimental resolution and are composed of four transitions, the symmetric and asymmetric NH_2^+ stretches and the phenol and C_β OH stretches at 3215 cm^{-1}, 3238 cm^{-1}, 3645 cm^{-1} and 3655 cm^{-1}, respectively. These modes have been assigned through comparison with the simulated spectra of the low energy conformers of $SyneH^+$. As already noted by Stearn *et al.*[31] in the case of protonated tyrosine, the orientation of the lone pair of the phenol hydroxyl does not affect the vibrational spectrum in the 3 µm region. So it is likely that the two spectra are to be assigned to the same conformer but the two rotamers along the OH orientation with respect to the phenyl ring (see also below).

The signal-to noise ratio of the IR-UV spectra being rather weak in the N-H stretching region, the IR beam has been more tightly focused in the center of the 3D-QIT trap with a 350 mm lens. In this condition, we have detected an IR photodissociation signal, corresponding to the

loss of H_2O, without UV laser (Figure S1). Water loss is the main fragmentation channel under low energy collisions in the ground state. In protonated Threonine, H_2O elimination proceeds through a proton transfer to the side chain hydroxyl leading to the aziridine structure.[32] The same mechanism is expected to occur in SyneH$^+$.

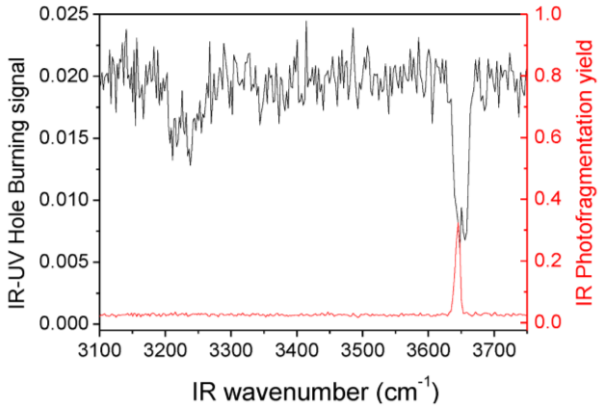

Figure 3. IR photodissociation spectrum (red line, right vertical axis) compared to IR-UV HB spectrum (black line) of SyneH$^+$. The IRPD spectrum is not conformer-selective but only works for the phenol hydroxyl mode with high efficiency (30%).

The IRPD spectrum of SyneH$^+$ is reported in Figure 3 and compared to the IR-UV HB spectrum reported in Figure 2. Two striking results are readily observed. First, the IR photofragmentation yield is in the order of 30%, so at least one order of magnitude larger than the UV photodissociation yield (about 2%). For both spectra, the reported fragmentation yields correspond to the signal of the fragment ions divided by the sum of the parent and fragment ions signal. Second, IR photodissociation is mode-specific: only the OH stretch mode of the phenyl ring at 3645 cm^{-1} is observed, while the Cβ-OH stretch, only 10 cm^{-1} further to the blue, is totally absent together with the two NH_2^+ modes which also display the so-called IRMPD transparency.[33]

3.2. Computational Analysis

3.2.1. Isomer Structures, Energies and Frequencies.

The ground state energy and the vibrational frequencies of SyneH$^+$ for the syn rotamer, calculated at the DFT/B97-D3/TZVPP level, are reported in Table 1. The structures of the syn rotamers of the low-energy conformers are reported in Figure 4. The anti rotamers (NH_2^+

group in anti position compared to the oxygen lone pair of the phenol hydroxyl) are in average 0.15 kcal/mol higher in energy compared to the syn rotamer for all conformers. Such small energy difference is within the error of the theoretical method. The vibrational frequencies of the syn and anti rotamers of the same conformer do not differ by more than 2-3 cm^{-1} and this small difference cannot allow for rotamer discrimination by their IR spectrum. In the following we discuss the results only for the syn rotamers.

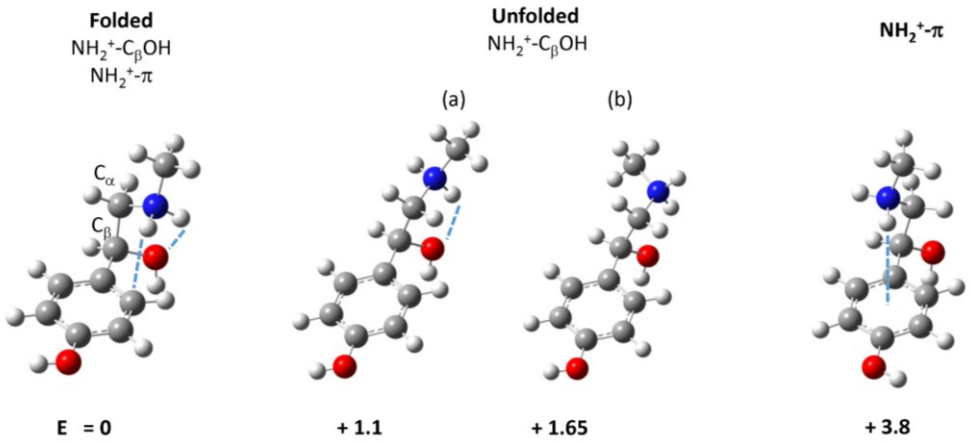

Figure 4. Structures and Energy (in kcal/mol) of the low energy syn conformers of SyneH$^+$.

Table 1. Relative ZPE-corrected ground-state energies and vibrational frequencies of the low energy conformers of SyneH$^+$ (syn rotamer) calculated at the DFT/B97-D3/TZVPP level. [a] The corresponding anti conformers are in average 0.15 kcal/mol higher in energy.

	E+ZPE	Cβ-OH	Ph-OH	NH_2 asym	NH_2 sym
Exp freq		3655	3645	3238	3215
Folded	0	3648 *(60)*	3638 *(64)*	3271 *(64)*	3208 *(60)*
Unfolded a	1.1	3651 *(104)*	3638 *(104)*	3316 *(105)*	3225 *(104)*
Unfolded b	1.65	3652 *(78)*	3638 *(52)*	3329 *(67)*	3215 *(48)*
NH_2-π	3.8	3642 *(128)*	3635 *(77)*	3304 *(70)*	3168 *(179)*

[a] Energy in kcal/mol. Frequencies in cm^{-1}. Frequency intensities (km/mol) in parenthesis.

The NH_2-π conformer lies 3.8 kcal/mol higher in energy compared to the global minimum, with calculated frequencies that show the largest deviations from the experimental values and can thus be discarded. The unfolded conformations are 1.1 and 1.65 kcal/mol higher in energy, in which the protonated NH_2 group forms an H-bond with the accepting Cβ-OH moiety. For the lowest energy conformer, noted folded, the NH_2 interacts as a proton donor both with the Cβ-

OH and the π cloud of the aromatic ring. This conformer indeed provides the best agreement with the experimental values, in particular for the asymmetric NH_2 stretch. Its calculated frequency is still overestimated by 33 cm^{-1} but those of the two unfolded conformers are 76 cm^{-1} and 91 cm^{-1} to the blue. The simulated vibrational spectra of all conformers are reported in Figure S2.

3.2.2. Excited state calculations

As already stated, the two syn/anti rotamers of the folded conformer cannot be discriminated by their IR spectrum. Nevertheless we have already shown, in the case of protonated tyrosine[15] and tyramine[22], that such rotamers can be assigned through a comparison with the adiabatic excitation energies calculated at the CC2 level. Geometry optimization and frequency calculations at the CC2/aug-cc-pVDZ level have thus been performed on the ground and first excited electronic states of $SyneH^+$ in the folded and unfolded structures in order to assign the vibronic spectrum. The results are reported in Table 2. The simulated Franck-Condon spectra of the folded conformers (syn and anti rotmers) are reported in Figure S3.

Table 2. Calculated adiabatic excitation energies (CC2/aug-cc-pVDZ) of the $\pi\pi^*$ state of the lowest energy conformers of $SyneH^+$ for the syn and anti rotamers.[a]

Conformer	Rotamer	$0_0^{0\ calc}$	$0_0^{0\ exp}$	$\Delta E^{(calc-exp)}$
Folded	Syn	34 930	35 406	- 475
	Anti	35 045	35 509	- 463
	$\Delta E_{Syn/Anti}$	115	103	8
Unfolded a	Syn	35 860	35 406	454
	Anti	35 833	35 509	324
	$\Delta E_{Syn/Anti}$	-27	103	130

[a] ZPE-corrected. All values in cm^{-1}.

For all conformers, the first excited state is a $\pi\pi^*$ transition, with a calculated ZPE-corrected adiabatic transition energy of 34 930 cm^{-1} and 35 045 cm^{-1}, for the syn and anti folded rotamers, respectively. The calculated absolute values are only underestimated by about 500 cm^{-1}, the agreement with the experimental values is noteworthy for the relative energy between the two rotamers of the folded conformer. The calculated adiabatic 0_0^0 excitation energies of the two rotamers differ by 115 cm^{-1}, the syn rotamer having the reddest band origin, while the experimental splitting is 103 cm^{-1}. These results are totally consistent with

the absolute errors found at the same level of theory in related systems, *i.e.* protonated tyrosine and tyramine.[15,22] For these two systems, the average deviation from the experimental value of the adiabatic excitation energy is - 539 cm^{-1} and the syn/anti splitting is 127 cm^{-1}. Thus, we can confidently assign the two UV-UV HB spectra of $SyneH^+$ to the syn and anti rotamers of the folded conformer. The two unfolded conformers have almost the same excitation energies and we only present the result of conformer a (see notation in table 2 and Figure 4). For the syn and anti rotamers of the unfolded conformer, the adiabatic excitation energies are calculated about 1000 cm^{-1} above the syn folded conformer. Besides, the energy splitting of the calculated adiabatic transition is -27 cm^{-1}, the anti rotamer having the reddest excitation energy.

It should be noted that the antibonding $\pi*$ orbital shows a partial electron transfer from the aromatic ring toward the protonated NH group pointing to the aromatic carbon atom (figure S4). In the $\pi\pi^*$ optimized structure, this induces a N-H bond lengthening of 0.017 Å and a slight puckering of the aromatic ring (dihedral angle 10 °) at the proton acceptor carbon. As for the protonated aromatic amino acids,[34,35] excited state proton transfer from the protonated amino group to the aromatic ring could occur, leading to UV specific photofragments induced by the C_α-C_β bond cleavage, which is indeed experimentally observed. It should be stressed that for the unfolded conformer, such proton transfer from the NH_2 group to the aromatic ring cannot obviously occur, which reinforces the initial structural assignment.

The second excited state is a $\pi\sigma^*$ state, in which the electron density is delocalized in an antibonding σ^* orbital of the protonated group. The S_2 state is calculated 0.9 eV higher in energy at the S1 $\pi\pi^*$ state optimized structure. The S_2 optimized structure leads to a slight change of the electron density of the σ^* orbital which now closely resembles a Rydberg orbital centered on the N-H bond. Its calculated adiabatic transition energy lies 0.5 eV above the $\pi\pi^*$ band origin. Experimentally, no H-loss reaction has been evidenced in the UV photofragmentation mass spectrum and the fragmentation branching ratio does not change with the excess energy brought by the UV excitation up to 2000 cm^{-1} above the band origin. So, it is concluded that the $\pi\sigma^*$ state is not involved in the deactivation process of $SyneH^+$ excited in the S_1 $\pi\pi^*$ state.

3.3. IR Photodissociation (IRPD) *vs* UV-PD and IR-UV Hole Burning Spectroscopy

The first striking result is that the IR fragmentation yield is ten-to-thirty times larger than the UV PD yield. As already reported in previous UV PID experiment, the UV fragmentation yield is weak, most of the time lower than one percent (see figure S1). Note that, following electronic excitation, many deactivation channels are in competition (radiative, IC, ISC, fragmentation), while in IR photoexcitation, neglecting the black body radiation occurring at much longer time than the ns-µs-ms time scales of the experiment, the only deactivation process is fragmentation following IVR. Besides, FC activities can dramatically affect the UV excitation efficiency, while IR absorption is strong in the 3 µm region.

In almost all the reported IRPD spectroscopic studies of bare amino acids or related compounds in the 3 µm region and although O-H and N-H stretches have similar linear absorption intensities, only the free X-H modes which are not involved in hydrogen bonding are clearly observed.[36–40] For these high frequency modes, IVR timescales are much faster than the laser pulse width (10 ns). Besides, IVR timescales are even shorter for the modes involved in H-bond, so anharmonicity effect cannot explain the missing lines in the IRPD spectra. Note that mode-specific fragmentation has been observed in the IRPD spectrum of NH_4^+-H_2O, the asymmetric OH stretch being much weaker than the corresponding symmetric stretch.[41] In this particular case, a simple and elegant mechanistic picture allows explaining the experimental finding. The oxygen atom moves along the dissociation coordinate upon symmetric OH excitation, thus directly weakening the intermolecular bond, while excitation of the asymmetric OH stretch moves the oxygen perpendicularly to the intermolecular bond. Mode-specific IRMPD efficiency has also been discussed in the case of hydrated alkali ion and sulfuric acid anion clusters.[33,42] In these clusters without symmetry, the mechanistic model cannot explain the results. The authors have proposed a more likely mechanism, emphasizing the large frequency change of the probed mode with the increase of the internal energy, as a result of an isomerization early in the IRPD process. Such out-of-resonance events should be particularly important for modes involved in H-bond and thus preventing multiphoton process to occur.

For all SyneH$^+$ conformers, the NH_2^+ group is involved in single or double hydrogen bond. Its stretching frequencies largely differ by up to 50 cm^{-1} depending on the conformer, as reported in Table 1. For each conformer, following the absorption of a first photon resonant with the

NH_2^+ stretching mode, the increase of internal energy will first induce an isomerization. In another conformation, the next photon will be out-of-resonance and the multiphoton absorption process will thus be quenched. The NH_2 asymmetric and symmetric stretching modes are indeed not observed through IRPD. On the contrary, the frequency of the phenol OH stretch, which is not involved in any intramolecular interaction, is conformer independent within 3 cm^{-1} of the calculated frequency of the folded conformer. Multiphoton absorption will thus be effective until the dissociation limit is reached, as experimentally observed. For the C_β-OH stretch, the calculated frequency of the folded conformer does not differ by more than 6 cm^{-1} as compared to the other ones, so multiphoton absorption should still occur during or after isomerization in the early step of the IRPD process. The only difference between the two hydroxyl modes is that this C_β-OH is a proton acceptor group for a weak intramolecular H-bond, at least in the two lowest-energy (folded and unfolded a) conformations, while the phenol OH is always free. The 100% IRPD transparency observed for the side chain hydroxyl mode indicates that this subtle structural property may induce larger spectral shifts as the internal energy increases as those predicted for the optimized structures. To try to further understand why the two OH stretching modes behave so differently with respect to IRPD would need additional works. In particular, we wish to record the conformer-selected IR spectrum (IR-UV HB) of the other low energy conformers of $SyneH^+$ through an IR hole-filing method followed by He cooling.[43] The small predicted frequency shifts of the C_β-OH stretch will thus be compared to the experimental values. It would also be instructive to perform quantum chemistry dynamics calculations to test if the H-bond and the potential proton transfer from the protonated amino group to the acceptor C_β-OH hydroxyl can lead to the quenching of successive IR photon absorption at the initial resonance frequency. Finally, *ab initio* molecular dynamics simulations[37] run at different temperatures should reveal the isomerization and the corresponding frequency shifts of the X-H stretching modes assumed during the IRPD process.

4. Conclusions

The UV and IR photodissociation spectroscopies of cold $SyneH^+$ have been performed in a cryogenically cooled Paul ion trap. Although two main families of conformers of low energy are predicted, only the folded structure is observed. Syn/anti rotamers along the phenol hydroxyl group are clearly assigned through the vibronic spectrum and excited state

calculations, while their experimental and predicted ground state vibrational spectra are undistinguished. The striking result of this study is the total IRPD transparency for all modes involved in hydrogen bond, even for the weak proton acceptor C_β-OH, while IR-UV HB spectroscopy recovers the entire spectra in the X-H stretching region. Such result, obtained with the same experimental setup, provides stringent evidence for isomerization during the multiphoton process within the 10 ns laser pulse as needed to induce IR photodissociation. Further works are planned to investigate the IRPD process, in particular the temperature and the laser power dependency.

Associated content

Supporting information

UV and IR photodissociation mass spectra of SyneH$^+$, simulated IR spectrum of the low energy conformers of SyneH$^+$, Franck-Condon spectra of SyneH$^+$ folded syn/anti, molecular orbitals of the S_1 and S_2 excited states of SyneH$^+$. The Supporting Information is available free of charge on the ACS Publications website at DOI:xxx

Acknowledgment

We acknowledge the use of the computing facility clusters MésoLUM of the LUMAT federation (FRLUMAT 2764) and MAGI of the University Paris 13.

References

(1) Arbo, M. D.; Larentis, E. R.; Linck, V. M.; Aboy, A. L.; Pimentel, A. L.; Henriques, A. T.; Dallegrave, E.; Garcia, S. C.; Leal, M. B.; Limberger, R. P. Concentrations of P-Synephrine in Fruits and Leaves of Citrus Species (Rutaceae) and the Acute Toxicity Testing of Citrus Aurantium Extract and P-Synephrine. *Food Chem. Toxicol.* **2008**, *46*, 2770–2775.

(2) Zucchi, R.; Chiellini, G.; Scanlan, T. S.; Grandy, D. K. Trace Amine-Associated Receptors and Their Ligands. *Br. J. Pharmacol.* **2006**, *149*, 967–978.

(3) Torp, K. D.; Tschakovsky, M. E.; Halliwill, J. R.; Minson, C. T.; Joyner, M. J. β-Receptor Agonist Activity of Phenylephrine in the Human Forearm. *J. Appl. Physiol.* **2001**, *90*, 1855–1859.

(4) Ishiuchi, S.; Asakawa, T.; Mitsuda, H.; Miyazaki, M.; Chakraborty, S.; Fujii, M. Gas-Phase

Spectroscopy of Synephrine by Laser Desorption Supersonic Jet Technique. *J. Phys. Chem. A* **2011**, *115*, 10363–10369.

(5) Wako, H.; Ishiuchi, S.; Kato, D.; Féraud, G.; Dedonder-Lardeux, C.; Jouvet, C.; Fujii, M. A Conformational Study of Protonated Noradrenaline by UV–UV and IR Dip Double Resonance Laser Spectroscopy Combined with an Electrospray and a Cold Ion Trap Method. *Phys. Chem. Chem. Phys.* **2017**, *19*, 10777–10785.

(6) Oomens, J.; Sartakov, B. G.; Meijer, G.; von Helden, G. Gas-Phase Infrared Multiple Photon Dissociation Spectroscopy of Mass-Selected Molecular Ions. *Int. J. Mass Spectrom.* **2006**, *254*, 1–19.

(7) MacAleese, L.; Maître, P. Infrared Spectroscopy of Organometallic Ions in the Gas Phase: From Model to Real World Complexes. *Mass Spectrom. Rev.* **2007**, *26*, 583–605.

(8) Grégoire, G.; Gaigeot, M. P.; Marinica, D. C.; Lemaire, J.; Schermann, J. P.; Desfrançois, C. Resonant Infrared Multiphoton Dissociation Spectroscopy of Gas-Phase Protonated Peptides. Experiments and Car–Parrinello Dynamics at 300 K. *Phys. Chem. Chem. Phys.* **2007**, *9*, 3082–3097.

(9) Dopfer, O.; Olkhov, R. V.; Maier, J. P. Microsolvation of HN 2 + in Argon: Infrared Spectra and Ab Initio Calculations of Ar N −HN 2 + (N = 1−13). *J. Phys. Chem. A* **1999**, *103*, 2982–2991.

(10) Gregoire, G.; Velasquez, J.; Duncan, M. . Infrared Photodissociation Spectroscopy of Small Fe+–(CO2)n and Fe+–(CO2)nAr Clusters. *Chem. Phys. Lett.* **2001**, *349*, 451–457.

(11) Solcà, N.; Dopfer, O. Protonated Benzene: IR Spectrum and Structure of C6H7. *Angew. Chemie Int. Ed.* **2002**, *41*, 3628–3631.

(12) Walters, R. S.; Pillai, E. D.; Duncan, M. A. Solvation Dynamics in Ni + (H 2 O) N Clusters Probed with Infrared Spectroscopy. *J. Am. Chem. Soc.* **2005**, *127*, 16599–16610.

(13) Maitre, P.; Lemaire, J.; Scuderi, D. Structural Characterization under Tandem Mass Spectrometry Conditions: Infrared Spectroscopy of Gas Phase Ions. *Phys. Scr.* **2008**, *78*, 58111.

(14) Kopysov, V.; Makarov, A.; Boyarkin, O. V. Nonstatistical UV Fragmentation of Gas-Phase Peptides Reveals Conformers and Their Structural Features. *J. Phys. Chem. Lett.* **2016**, *7*, 1067–1071.

(15) Féraud, G.; Broquier, M.; Dedonder, C.; Jouvet, C.; Grégoire, G.; Soorkia, S. Excited State Dynamics of Protonated Phenylalanine and Tyrosine: Photo-Induced Reactions Following

Electronic Excitation. *J. Phys. Chem. A* **2015**, *119*, 5914–5924.

(16) Garcia, R. L.; Nieuwjaer, N.; Desfrançois, C.; Lecomte, F.; Leite, S. D.; Manil, B.; Broquier, M.; Grégoire, G. Vibronic Spectra of Protonated Hydroxypyridines: Contributions of Prefulvenic and Planar Structures. *Phys. Chem. Chem. Phys.* **2017**, *19*, 8258–8268.

(17) Seaiby, C.; Zabuga, A. V; Svendsen, A.; Rizzo, T. R. IR-Induced Conformational Isomerization of a Helical Peptide in a Cold Ion Trap. *J. Chem. Phys.* **2016**, *144*, 14304.

(18) DeBlase, A. F.; Harrilal, C. P.; Lawler, J. T.; Burke, N. L.; McLuckey, S. A.; Zwier, T. S. Conformation-Specific Infrared and Ultraviolet Spectroscopy of Cold [YAPAA+H] + and [YGPAA+H] + Ions: A Stereochemical "Twist" on the β-Hairpin Turn. *J. Am. Chem. Soc.* **2017**, *139*, 5481–5493.

(19) Choi, C. M.; Choi, D. H.; Heo, J.; Kim, N. J.; Kim, S. K. Ultraviolet-Ultraviolet Hole Burning Spectroscopy in a Quadrupole Ion Trap: dibenzo[18]crown-6 Complexes with Alkali Metal Cations. *Angew. Chem. Int. Ed. Engl.* **2012**, *51*, 7297–7300.

(20) Kang, H.; Féraud, G.; Dedonder-Lardeux, C.; Jouvet, C. New Method for Double-Resonance Spectroscopy in a Cold Quadrupole Ion Trap and Its Application to UV–UV Hole-Burning Spectroscopy of Protonated Adenine Dimer. *J. Phys. Chem. Lett.* **2014**, *5*, 2760–2764.

(21) Féraud, G.; Dedonder, C.; Jouvet, C.; Inokuchi, Y.; Haino, T.; Sekiya, R.; Ebata, T. Development of Ultraviolet–Ultraviolet Hole-Burning Spectroscopy for Cold Gas-Phase Ions. *J. Phys. Chem. Lett.* **2014**, *5*, 1236–1240.

(22) Broquier, M.; Soorkia, S.; Grégoire, G. A Comprehensive Study of Cold Protonated Tyramine: UV Photodissociation Experiments and Ab Initio Calculations. *Phys. Chem. Chem. Phys.* **2015**, *17*, 25854–25862.

(23) TURBOMOLE V6.6, a Development of University of Karlsruhe and Forschungszentrum Karlsruhe GmbH, 1989-2007, TURBOMOLE GmbH, since 2007; Available from http://www.turbomole.com.

(24) Ahlrichs, R. Efficient Evaluation of Three-Center Two-Electron Integrals over Gaussian Functions. *Phys. Chem. Chem. Phys.* **2004**, *6*, 5119–5121.

(25) Köhn, A.; Hättig, C. Analytic Gradients for Excited States in the Coupled-Cluster Model CC2 Employing the Resolution-of-the-Identity Approximation. *J. Chem. Phys.* **2003**, *119*, 5021–5036.

(26) Kendall, R. A.; Dunning, T. H.; Harrison, R. J. Electron Affinities of the First-row Atoms Revisited. Systematic Basis Sets and Wave Functions. *J. Chem. Phys.* **1992**, *96*, 6796–6806.

(27) Grimme, S. Semiempirical GGA-Type Density Functional Constructed with a Long-Range Dispersion Correction. *J. Comput. Chem.* **2006**, *27*, 1787–1799.

(28) Schäfer, A.; Huber, C.; Ahlrichs, R. Fully Optimized Contracted Gaussian Basis Sets of Triple Zeta Valence Quality for Atoms Li to Kr. *J. Chem. Phys.* **1994**, *100*, 5829–5835.

(29) Grimme, S.; Ehrlich, S.; Goerigk, L. Effect of the Damping Function in Dispersion Corrected Density Functional Theory. *J. Comput. Chem.* **2011**, *32*, 1456–1465.

(30) Gloaguen, E.; Pollet, R.; Piuzzi, F.; Tardivel, B.; Mons, M. Gas Phase Folding of an (Ala)4 Neutral Peptide Chain: Spectroscopic Evidence for the Formation of a β-Hairpin H-Bonding Pattern. *Phys. Chem. Chem. Phys.* **2009**, *11*, 11385–11388.

(31) Stearns, J. A.; Mercier, S.; Seaiby, C.; Guidi, M.; Boyarkin, O. V.; Rizzo, T. R. Conformation-Specific Spectroscopy and Photodissociation of Cold, Protonated Tyrosine and Phenylalanine. *J. Am. Chem. Soc.* **2007**, *129*, 11814–11820.

(32) O'Hair, R. A. J.; Reid, G. E. Does Side Chain Water Loss from Protonated Threonine Yield N-Protonated Dehydroamino-2-Butyric Acid? *Rapid Commun. Mass Spectrom.* **1998**, *12*, 999–1002.

(33) Yacovitch, T. I.; Heine, N.; Brieger, C.; Wende, T.; Hock, C.; Neumark, D. M.; Asmis, K. R. Vibrational Spectroscopy of Bisulfate/Sulfuric Acid/Water Clusters: Structure, Stability, and Infrared Multiple-Photon Dissociation Intensities. *J. Phys. Chem. A* **2013**, *117*, 7081–7090.

(34) Grégoire, G.; Jouvet, C.; Dedonder, C.; Sobolewski, A. L. Ab Initio Study of the Excited-State Deactivation Pathways of Protonated Tryptophan and Tyrosine. *J. Am. Chem. Soc.* **2007**, *129*, 6223–6231.

(35) Grégoire, G.; Lucas, B.; Barat, M.; Fayeton, J. A.; Dedonder-Lardeux, C.; Jouvet, C. UV Photoinduced Dynamics in Protonated Aromatic Amino Acid. *Eur. Phys. J. D* **2009**, *51*, 109–116.

(36) Crestoni, M. E.; Chiavarino, B.; Scuderi, D.; Di Marzio, A.; Fornarini, S. Discrimination of 4-Hydroxyproline Diastereomers by Vibrational Spectroscopy of the Gaseous Protonated Species. *J. Phys. Chem. B* **2012**, *116*, 8771–8779.

(37) Schindler, B.; Joshi, J.; Allouche, A.-R.; Simon, D.; Chambert, S.; Brites, V.; Gaigeot, M.-P.;

Compagnon, I. Distinguishing Isobaric Phosphated and Sulfated Carbohydrates by Coupling of Mass Spectrometry with Gas Phase Vibrational Spectroscopy. *Phys. Chem. Chem. Phys.* **2014**, *16*, 22131–22138.

(38) Patrick, A. L.; Stedwell, C. N.; Schindler, B.; Compagnon, I.; Berden, G.; Oomens, J.; Polfer, N. C. Insights into the Fragmentation Pathways of Gas-Phase Protonated Sulfoserine. *Int. J. Mass Spectrom.* **2015**, *379*, 26–32.

(39) Paciotti, R.; Coletti, C.; Re, N.; Scuderi, D.; Chiavarino, B.; Fornarini, S.; Crestoni, M. E.; Caer, S. Le; Ortega, J. M.; Glotin, F.; et al. Serine O-Sulfation Probed by IRMPD Spectroscopy. *Phys. Chem. Chem. Phys.* **2015**, *17*, 25891–25904.

(40) Jeanne Dit Fouque, K.; Lavanant, H.; Zirah, S.; Steinmetz, V.; Rebuffat, S.; Maître, P.; Afonso, C. IRMPD Spectroscopy: Evidence of Hydrogen Bonding in the Gas Phase Conformations of Lasso Peptides and Their Branched-Cyclic Topoisomers. *J. Phys. Chem. A* **2016**, *120*, 3810–3816.

(41) Pankewitz, T.; Lagutschenkov, A.; Niedner-Schatteburg, G.; Xantheas, S. S.; Lee, Y.-T. Infrared Spectrum of NH4+(H2O): Evidence for Mode Specific Fragmentation. *J. Chem. Phys.* **2007**, *126*, 74307.

(42) Beck, J. P.; Lisy, J. M. Infrared Spectroscopy of Hydrated Alkali Metal Cations: Evidence of Multiple Photon Absorption. *J. Chem. Phys.* **2011**, *135*, 44302.

(43) Dian, B. C.; Longarte, A.; Winter, P. R.; Zwier, T. S. The Dynamics of Conformational Isomerization in Flexible Biomolecules. I. Hole-Filling Spectroscopy of N-Acetyl Tryptophan Methyl Amide and N-Acetyl Tryptophan Amide. *J. Chem. Phys.* **2004**, *120*, 133–147.

TOC graphic:

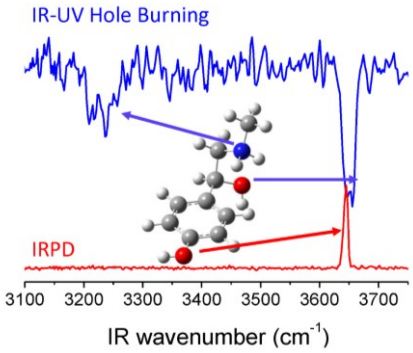
IR-UV Hole Burning
IRPD
3100 3200 3300 3400 3500 3600 3700
IR wavenumber (cm-1)